Title

Assessment of Embryonic Bioactivity through Changes in the Water Structure Using Near-Infrared Spectroscopy and Imaging

Author(s)

Mika Ishigaki, Yui Yasui, Misato Kajita, and Yukihiro Ozaki

Journal

Analytical Chemistry 2020, 92, 12, 8133–8141

Published

May 14, 2020

URL

https://pubs.acs.org/doi/10.1021/acs.analchem.0c00076

Assessment of embryonic bioactivity through changes in the water structure using near-infrared (NIR) spectroscopy and imaging

Mika Ishigaki,[1,2]* Yui Yasui,[3] Misato Kajita,[3] Yukihiro Ozaki[3]

[1]*Raman Project Center for Medical and Biological Applications, Shimane University, 1060 Nishikawatsu, Matsue, Shimane 690-8504, Japan*

[2]*Faculty of Life and Environmental Sciences, Shimane University, 1060 Nishikawatsu, Matsue, Shimane 690-8504, Japan*

[3]*School of Science and Technology, Kwansei Gakuin University, 2-1 Gakuen, Sanda, Hyogo 669-1337, Japan*

*Authors to whom correspondence should be sent.

*E-mail: ishigaki@life.shimane-u.ac.jp (M.I.)

Abstract

We explored the influence of embryonic bioactivity on the water structure using near-infrared (NIR) spectroscopy and imaging. Four groups of Japanese medaka fish (*Oryzias latipes*) eggs were studied: (a) one group of eggs was activated by fertilization, and (b)-(d) three groups of eggs were non-activated because embryogenesis was stopped or not started by (b) culturing under cold temperature, (c) instant freezing or (d) the lack of fertilization. The yolks of the activated eggs contained higher proportions of weakly hydrogen bonded water than those of non-activated eggs. A possible factor responsible for the significant changes in the water structure was revealed to be a protein secondary structural change from an α-helix to a β-sheet in the activated eggs. NIR images of the activated eggs successfully visualized the water structural variation in the yolk with a higher proportion of weak hydrogen bonds due to the activation of embryonic development. The embryogenic activity could be assessed through the water hydrogen bond network, which is affected by newly generated proteins with different secondary structures.

Keywords: Bioactivity, Embryogenesis, Water structure, NIR spectroscopy, NIR imaging

Introduction

The mechanism of the birth of life is mysterious and still attracts considerable interest of humanity. The development of animals is initiated by fertilization, and various proteins are synthesized by gene expression. The developmental process is precisely controlled by the production of the required RNAs and proteins precisely when they are needed. Studies in various research fields such as genome analysis, proteomics, the specific amplification of RNA, the library construction of cDNA, and fluorescence staining have been conducted to elucidate the phenomenon of birth.[1-5] These technologies enable the unraveling of embryogenesis at the molecular level. However, these methods are basically destructive or invasive, and it remains challenging to explore material variations in embryos *in situ* at the molecular level and in a noninvasive manner. Therefore, the aim of our present study is to disclose the process of life birth *in situ* while keeping embryos alive without staining.

Near-infrared (NIR) spectroscopy is a vibrational spectroscopy that is similar to infrared (IR) and Raman spectroscopies.[6, 7] In the NIR wavelength region, absorbance bands due to the overtone and combination modes of molecular vibrations, the so-called forbidden transitional modes, are observed.[6, 7] Therefore, the NIR region has an advantage with respect to the permeability over the visible (Vis) and infrared (IR) regions. In particular, a small disturbance due to water absorption in the NIR region enables nondestructive and noninvasive studies of aqueous samples on the order of millimeters in thickness, while in the mid-IR region, samples on the order of micrometers can be investigated.[6-11] As a Raman band due to water, the intensity of the O-H bending mode at 1650 cm^{-1} is weak, and the contribution is hidden in the amide I region near 1650 cm^{-1}.[12, 13] Moreover, the symmetric and asymmetric O-H stretching modes appearing at 3250 and 3400 cm^{-1}, respectively, are difficult to detect with high accuracy because of a decrease in the detector sensitivity.[13] Therefore, Raman spectroscopy has some difficulties enclosing the structure of biological water *in situ*. That is, NIR spectroscopy is suggested to be the only way to investigate water and proteins simultaneously *in situ.* Water is the main component of biological

samples. The biological reactions occur within aqueous solutions, and the effects of these reactions should be reflected in the structure of water. The concentration gradient of biomolecules and their molecular structure also affect the water structure through hydrogen bonds. Therefore, metabolic activity caused by gene expression, which promotes protein production or protein structural changes, is expected to be measurable through variations in the water structure using NIR spectroscopy and imaging.

The structure of water is one of the most basic scientific issues studied experimentally and theoretically by many research groups for nearly a century; however, it has not yet been fully elucidated.[14] The two major models for water structure are as follows: (1) water is a mixture of different components,[15-20] and (2) water is a continuum system in which hydrogen bonds are continuously varied.[22, 22] Vibrational spectroscopies, such as IR, Raman, and NIR spectroscopies, support the former model. According to these techniques, water consists mainly of two components, namely, weakly hydrogen bonded (WHB) and strongly hydrogen bonded (SHB) water.[15-20] Šašić et al. investigated the NIR spectra of water in the 1300-1600 nm region over a temperature range of 6–76 °C.[16] These researchers concluded that

more than 99% of the water spectra could be explained by only two species of water (WHB and SHB water).[16] Czarnik-Matusewicz et al. also analyzed water structural variations due to a temperature variation in the range of 25–80 °C using the NIR (8000–4000 cm^{-1}) and mid-IR (MIR, 4000–2590 cm^{-1}) regions.[17] The results revealed the presence of two spectral components that individually changed depending on the temperature variation.[17] A Raman study of water in the range of -23–45 °C also showed two main structural forms of water.[20]

NIR imaging has been a matter of keen interest because it provides the nondestructive spatial distribution of chemical components, even for thick materials.[23, 24] This method has been used for a variety of applications including the quality evaluation of foods and pharmaceutical tablets, the diffusion process of solvents in tablets and polymers, and the component and crystallinity distributions of polymers.[6-8, 25] In our previous studies, the embryogenesis of fish eggs was investigated as an application of NIR imaging in biology.[26-30] The relative content of proteins and lipids drastically changed on the day just before hatching, which enabled the prediction of hatching on the next day with a higher than 99% accuracy.[26] Furthermore,

owing to the metabolic changes within egg yolks, the proteins with α-helix- or β-sheet-rich structures clearly showed different variation patterns during the course of egg development.[28] Using a newly developed Fourier transform (FT)-NIR imaging system with a partial movable mirror, heartbeat signals of fish egg embryos were extracted, which enabled the visualization of the blood flow of a fish egg *in vivo* in addition to the biomolecular distribution of water, proteins, and lipids.[30]

In the present study, the influence of embryonic bioactivity on the water structure was investigated for Japanese medaka fish (*Oryzias latipes*) eggs using NIR spectroscopy and imaging. The variations in the egg yolk components, such as proteins, lipids, and water, were investigated. These variations were compared among four different groups of egg samples: (a) the first group of eggs was activated by fertilization, and three groups of eggs were non-activated because embryogenesis was stopped or not started by (b) culturing under cold temperature, (c) instant freezing or (d) lack of fertilization. The proportion of WHB water in the yolks of activated eggs was higher than that in the non-activated eggs. A few characteristics that may influence the water structure, such as the temperature, ion concentration,

protein concentration, and protein secondary structural changes, were examined. A possible factor responsible for the significant changes observed in the water structure was the protein structural changes. The secondary structural change from an α-helix to a β-sheet was confirmed in the fish eggs via Raman spectroscopy. That is, embryonic activity could be assessed through the hydrogen bond network of water, which is affected by gene expression and newly generated proteins with different secondary structures. We aimed to better understand the differences between whether a new life will be born or not by investigating "water" as the main component of biology from the standpoint of molecular spectroscopy.

Materials and methods

Fish eggs

Fish eggs were obtained from adult Japanese medaka (*Oryzias latipes*). The fish were kept at a water temperature of 25 °C and spawned eggs in the morning. The egg size was approximately 1.5 mm in diameter. A fertilized egg contains three major components: an egg yolk, oil droplets, and a blastodisc, which develops into the fish body. Some eggs were unfertilized,

perhaps because of their low quality, although the reason was not identified. An unfertilized egg does not have a biased configuration as in a fertilized egg, and small oil droplets are scattered universally all over the egg.

In the present study, the variations in the components of the yolk, such as proteins, lipids, and water, were investigated and compared for four different kinds of egg samples: (a) eggs that were activated by fertilization and three kinds of non-activated eggs where embryogenesis was stopped or not started by (b) culturing under cold temperatures, (c) instant freezing or (d) the lack of fertilization. The eggs in group (a) were collected on the day of fertilization (FD) and showed normal egg development. Thus, these eggs were expected to have the highest metabolic activity. The eggs in group (b) were fertilized eggs that were collected on the FD and were incubated at 3 °C; their development was stopped. The eggs in group (c) were prepared by freezing the fertilized eggs that were collected on the FD with liquid nitrogen so that their living activity was stopped at that moment. NIR measurements of the eggs in group (c) were performed after they were thawed and retained at 25 °C. The eggs in group (d) were unfertilized and exhibited relatively low metabolic activity because there was no gene

expression due to egg development.

The study was approved by the ethics committee of Kwansei Gakuin University. The experiments were performed in accordance with the fundamental guidelines for proper conduct of animal experiments and related activities in academic research institutions under the jurisdiction of the Ministry of Education, Culture, Sports, Science and Technology in Japan.

NIR measurements

NIR measurements were performed in both point mode and imaging mode using a Perkin-Elmer (Waltham, MA) imaging system consisting of a Spectrum One FT-NIR spectrometer coupled to a Spectrum Spotlight 300 NIR microscope. In the point mode measurements, NIR absorbance spectra were recorded in the 7800-4000 cm^{-1} region at a 4 cm^{-1} spectral resolution, with an accumulation of 60 scans. To reduce individual variations and local dependencies, 10 NIR spectra were obtained from the yolk components per egg. The mean NIR absorbance spectra were calculated for each egg group after preprocessing the baseline correction. Second derivative spectra were calculated using the Savitzky-Golay method with 15 points. In the imaging

mode, NIR imaging data were measured in transmission mode over an area of 1.5 × 1.5 mm^2 with a pixel size of 25 × 25 μm^2 and a spectral resolution of 4 cm^{-1} by adding four scans for a spectrum in the 6200–4000 cm^{-1} region. To fix an egg for the NIR measurement, it was sandwiched between two glass slides with two pinch cocks. The space between the two glass slides was set at 0.36 mm using spacers. The distributions of biomaterials such as proteins, lipids, and water were visualized by plotting the intensities in the second derivative spectra of the notable peaks for each component, the wavenumber of the peak positions, and the data extracted by chemometrics methods. For spectral analysis, the chemometrics software Unscrambler X 10.2 (Camo Analytics, Oslo, Norway), OriginPro 6.1 (OriginLab Corporation, Massachusetts, USA), and Graph-R free software were used.

Sample preparation and NIR measurements in vitro

To quantitatively evaluate the magnitude of a water peak shift at approximately 5200 cm^{-1}, four kinds of perturbations were given to ultrapure water: (i) temperature, (ii) ion concentration, (iii) protein concentration, and (iv) the secondary structural changes of proteins. The protein reagents

albumin (OVA), β-lactoglobulin, and bovine serum albumin (BSA) were dissolved using 0.05 M Tris-HCl buffer. The detailed protocols for the sample preparation and NIR measurements are exhibited in the Supporting Information (SI) 1.

Results and discussion

Figure 1 depicts the mean NIR absorbance spectra in the 7800-4000 cm^{-1} region obtained from egg yolks of groups (a), (b), (c), and (d). Broad features due to water are observed at 7000 and 5200 cm^{-1}. These two bands are assigned to the combination of the antisymmetric and symmetric O-H stretching modes and that of the antisymmetric O-H stretching and O-H bending modes of water, respectively.[31] The second derivative of the spectra in Figure 1 in the 5000-4200 cm^{-1} region is exhibited in Figure 2A. Weak peaks due to the protein (4864, 4612, and 4538 cm^{-1}) and lipid (4410, 4340, 4258 cm^{-1}) components are observed. The peak at 4864 cm^{-1} is assigned to the combination modes of the N-H stretching vibration and amide II (amide A + II),[32, 33] and the peak at approximately 4612 cm^{-1} was due to the combination modes of amide A and amide III (amide A + III).[34] The peak at

4538 cm^{-1} is also ascribed to the amide modes relating to the β-sheet structure of proteins.[34, 35] The prominent peaks at 4338 and 4258 cm^{-1} arise from the combination modes of the C-H stretching and the bending modes of lipids or aliphatic compounds; the residual band at 4410 cm^{-1} also comes from lipids.[36, 37] In this way, NIR spectra allow us to probe the variations in water and in proteins and lipids at the same time.

A comparison of the second derivative intensities of these six peaks showed their decrements in the activated group (a) eggs and in the non-activated group (b) eggs at a low temperature (Figure 2B). Notably, the protein and lipid components decreased in groups (a) and (b) compared with those in the other two groups of non-activated eggs, (c) and (d). An egg yolk contains sufficient energy, such as proteins and lipids, for egg development and for after hatching until the first feeding.[38] Therefore, the decrease in the bands due to the proteins and lipids in groups (a) and (b) could be interpreted as the increased usage of yolk components in groups (a) and (b) for egg development. The degree of egg development of group (c) eggs seemed to be similar to that of group (b) eggs because the eggs in both groups started their development and then stopped it due to temperature stress. However,

the temperature stimulation was more intense in group (c) than in group (b). Since egg development in group (c) was rapidly stopped by liquid nitrogen, the damage to the eggs was likely to be serious. The unfertilized eggs in group (d) never started their development, and they did not consume their pre-stored energy, except for that to live by itself. Therefore, the eggs in groups (a) and (b) and those in groups (c) and (d) showed similar spectral variations regarding the proteins and lipids (Figure 2B).

Figure 3A depicts the second derivative spectra in the 5500-5000 cm^{-1} region of the four kinds of egg yolk groups. The water band at 5250 cm^{-1} seemed to have different spectral properties from that at approximately 5170 cm^{-1}, depending on egg groups (Figure 3A). To extract the different components characteristic for each egg group, principal component analysis (PCA) was carried out for the data set of the yolk second derivative spectra on all egg groups.[39] Figure 3B and 3C show the score and loading plots of principal component (PC) 1 and PC2, respectively. The dataset was roughly grouped into two groups as activated (a) or non-activated (b)-(d) eggs, and PC2 was used as the factor to discriminate between them (Figure 3B). The second derivative spectral feature due to water was observed in the loading

plot of PC1 (Figure 3C), and PC1 scores merely exhibited the variation in the peak intensities due to water. In contrast, the loading of PC2 showed a different spectral pattern compared with that of PC1, and it contained three peaks at 5336, 5276, and 5200 cm^{-1} (Figure 3C). Figure 3D exhibits the mean scores of PC2, and it revealed that the activated group (a) eggs had negative values of PC2 on average, which means that the water species represented by the loading plot of PC2 worked in a subtractive manner in egg group (a). Hence, the PCA result can be interpreted as a water band at approximately 5200 cm^{-1} shifting overall to a higher wavenumber in the activated group (a) than in the non-activated groups (b)-(d).

In the models of the water mixtures of different components, water consists of two main species at room temperature: SHB (dominant contribution at lower temperatures) and WHB (appearing at higher temperatures) water.[15, 16] Šašić et al. reported that temperature-dependent NIR spectra of water could be explained using these two components more than 99% of the time.[16] A follow-up experiment regarding the temperature-dependent NIR spectral variation of pure water was carried out. With an increase in the water temperature, the proportion of WHB water species

became higher, and the absorbance peak due to water at approximately 5250 cm^{-1} shifted to a higher wavenumber. The detailed data for the experiment are described in SI2. Therefore, the upward frequency shift of the water band in the activated eggs (a) can be interpreted as the proportion of WHB water species increasing due to the increase in egg bioactivity. To quantitatively evaluate the relative water contributions, two parameters were calculated: (1) the ratio of the second derivative intensity due to WHB and SHB water species and (2) the peak shift of the second derivative spectra at approximately 5250 cm^{-1}.

Evaluation of the relative contribution of WHB and SHB water species

(1) The ratio of the second derivative intensity

In the second derivative spectra in the 5500-5000 cm^{-1} region, a residual peak was observed at approximately 5170 cm^{-1} (Figure 3A). Based on the two structural models of water, the peaks at approximately 5250 and 5170 cm^{-1} corresponded to the WHB and SHB water components, respectively, as discussed in SI2. The assignment seems to be reasonable from the knowledge of the water structural transition shown by the temperature variation in the

NIR spectra.[16-19] Figure 4A shows the mean ratio of the second derivative intensity defined as I_{5250}/I_{5170} (WHB/SHB). In the activated eggs, the proportion of WHB water was significantly higher than that in the non-activated eggs (Figure 4A).

(2) Peak positions due to water absorption

Two bands due to the WHB and SHB water species overlapped in the 5500-5000 cm^{-1} region. Since these two absorption bands were close to each other, their intensities and positions were reflected to each other in the second derivative spectra. Therefore, the relative contributions of WHB and SHB were assessed by comparing their peak positions. To extract the peak positions of the second derivative spectra, these species were once more differentiated, and the point where the third derivative spectrum became 0 was read out. Figure 4B exhibits the peak position of WHB water for the four kinds of eggs in the second derivative spectra. The WHB peak at approximately 5250 cm^{-1} in the activated group (a) eggs had a higher frequency than those in the non-activated group (b)-(d) eggs by 2-4 cm^{-1}. Therefore, the upward frequency shift of the water band in the activated

group (a) could be interpreted as the relative proportion of WHB water within all water components being higher in the activated group (a) eggs than in the non-activated groups (b)-(d).

In this way, two parameters consistently showed higher contributions of WHB water species in the activated group (a) eggs than in the non-activated group (b)-(d) eggs. However, it was unclear whether the magnitude of the peak shifts was significant or not to discuss the influence of egg bioactivity. To further quantitatively evaluate the magnitude of the peak shift, the influences of the perturbations to the water structure were evaluated using simple in vitro systems, including (i) temperature, (ii) ion concentration, (iii) protein concentration, and (iv) the secondary structural changes of proteins.

In case (i), a change in the water temperature by 50 C° was needed to obtain a 2-4 cm^{-1} shift. The inner water temperature within the activated eggs was unlikely to change very much. For the changes in the ion concentration (ii), NaCl and Na_2SO_4 were selected because they have different anion ranking strengths expressed by the Hofmeister series as $SO_4^{2-} > ClO_4^- > I^- > Cl^-$.[40] The peak shifts of 2-4 cm^{-1} required 0.8∼1.0 M concentration changes

in the ions, and large changes in ion concentration truly do not seem feasible within living bodies. Similarly, the effect of the protein concentration (iii) on the water structure was investigated by varying the albumin concentration. The results revealed that more than a 20 wt% albumin concentration was required to induce a significant peak shift of water. Such large changes also cannot occur in real eggs. To assess the influence of the protein secondary structural changes (iv) on water, the thermal denaturation processes of OVA, β-lactoglobulin, and BSA were investigated. Above 70 °C, the protein secondary structure varied from an α-helix to a β-sheet, leading to the upward frequency shift of the water peak by 4-12 cm^{-1}. The albumin concentration was 8 wt% in the present in vitro experiment, and the weight percent concentration of proteins amounted to the order of some dozens of wt%, as discussed in SI3. Therefore, the protein structural transition was a candidate to induce significant water structural changes, and the phenomena could be detected using NIR spectroscopy *in vivo*.

With an increase in the proportion of β-sheets, the peak at approximately 4610 cm^{-1} shifted to a higher frequency in all three samples. The detailed experimental data and discussions regarding these denaturation

processes are summarized in SI4. Figure 5A and 5B plot band positions due to the water and proteins of three kinds of protein aqueous solutions at approximately 5250 and 4610 cm^{-1}, respectively. The band positions simultaneously varied with the secondary structural changes caused by thermal denaturation. In all cases, the upward frequency shifts of the peak at 4612 cm^{-1} were correlated with the upward shifts of the water band. That is, the proportion of WHB water was likely to be increased with a higher proportion of the β-sheet structure of protein. Wu et al. reported that the secondary structural changes of human serum albumin (HSA) from an α-helix to a β-sheet caused by heating induced an upward frequency shift of the water band at 7000 cm^{-1}, correlating with a higher frequency shift of the protein band at approximately 4612 cm^{-1}.[41] These researchers also concluded that water species with no or a small number of hydrogen bonds increased with the denaturation process because more hydrophobic residues, originally packed within the protein interior, were exposed to water.[41]

Second derivative spectra of the four kinds of fish eggs were also examined. The peak at 4615 cm^{-1} shifted by 2-4 cm^{-1} to a lower wavenumber in the activated group (a) eggs compared to those of the non-activated groups

(b)-(d) (Figure 2A). Judging simply from the results of the protein peak shift, the secondary structure seemed to change from a β-sheet to an α-helix due to activation of egg development. However, developmental activation generated a water shift at higher wavenumbers by 2-4 cm^{-1}. The relationship of the NIR band shifts between proteins and water in real eggs did not exactly correspond to that of the single protein structural changes from an α–helix to a β-sheet. The reason for the inconsistency may be that many kinds of proteins are in real living bodies. Each protein has a different frequency in the amide A + III mode at approximately 4616 cm^{-1}. Therefore, the protein components should at least be changed by gene expression after fertilization; the amide mode was downshifted in the activated eggs regardless of the protein secondary structural variations.

Investigation of the protein secondary structural changes in egg yolks using Raman spectroscopy

To confirm the possibility of protein secondary structural changes, a Raman spectroscopic study was carried out for the same egg groups (a)-(d) *in situ*. The variations in the peak intensity and peak shifts in the amide I (∼1660

cm^{-1}) and amide III (~ 1250 cm^{-1}) regions indicated that the relative proportion of the protein components with α-helix and β-sheet structures decreased and increased, respectively.[42] The detailed Raman results and discussions are demonstrated in SI5. The protein secondary structural changes with more β–sheets, as suggested by the Raman spectra, were consistent with the water structural variation with a higher proportion of WHB by NIR spectroscopy. The downward shift of the amide A+III mode at 4616 cm^{-1} in NIR second derivative spectra, accompanied by the secondary structural variation to increased β–sheets, is not inconsistent because different species of proteins are generated by gene expression after fertilization. Judging from the results of both NIR and Raman spectroscopies, proteins with a β-sheet-rich structure were increased after fertilization, and protein components were drastically changed. Protein synthesis and secondary structural variations affected the water structure, resulting in a higher proportion of WHB. This finding enabled us to conclude that the protein structures were changed by the activation of egg development and that the hydration of water was drastically changed by life activity.

NIR images expressing bioactivity of egg development

Figure 6A exhibits images of the four kinds of fish egg groups: eggs (a) activated by fertilization, (b) cultured at cold temperature, (c) experienced instant freezing, and (d) those that were not fertilized. Figure 6B-6D displays NIR images constructed by plotting the second derivative intensities of the bands at 4340, 4616, and 5856 cm^{-1}, which were due to the combination of C-H stretching and the bending modes of hydrocarbons and aliphatic compounds,[31, 37] the combination of amide A and II,[31, 43, 44] and the first overtone of the C-H stretching modes of the CH_2 groups in the lipid components,[31, 45, 46] respectively. In the activated group (a), three structures (a yolk, oil droplets, and a blastodisc) were clearly visualized in both bright field and NIR images, and their distributions were in good agreement with each other. The lipid and protein components were confirmed to be located in the yolk and less in the blastocyst, which would be an embryonic body, as shown in Figure 6B and 6C. Similar patterns of the chemical distributions were observed in groups (a) and (b). However, in egg group (c), the yolk and blastodisc looked indistinguishable, and the formed embryonic structures after fertilization were likely destroyed by the shock of liquid nitrogen. In

egg group (d), the oil droplets did not coalesce into a large droplet, and the blastodisc, of course, was not structured because the eggs were not fertilized. The concentration of C-H compounds was higher in the oil droplets, yolk and blastodisc, in descending order (Figure 6A). Moreover, the second derivative intensities at 4336 and 4612 cm^{-1} were decreased on average in groups (a) and (b) compared to groups (c) and (d) due to the energy consumption required for egg development (Figure 6B and 6C), as clarified in the point mode measurements (Figure 2B). The NIR images constructed by the peak intensity at 5856 cm^{-1}, which was assigned to the first overtone of C-H stretching modes in unsaturated fatty acids,[37, 45] made the structures of oil droplets and the thin egg membrane clear (Figure 6D).

To visualize the bioactivity of the fish eggs, the structural differences in water were visualized. The variations in the water structure were clarified by plotting the ratio of second derivative intensities of the water bands defined as I_{5170}/I_{5250} (Figure 6E). The reddish color in Figure 6E indicates that the ratio of SHB was higher. Therefore, in the non-activated eggs, the proportion of SHB water (~5170 cm^{-1}) was higher than that in the activated eggs. Figure 6F was developed by plotting the scores of PC2, as shown in Figure 3C. In

this case, higher values of PC2 scores (red color) corresponded to higher contributions of SHB water. In the non-activated eggs, especially for the group (d) eggs, the egg components, on the whole, had higher PC2 values, indicating that the contribution of SHB water was higher in the group (d) eggs than in the activated group (a) eggs. NIR images constructed by the peak position due to WHB water (~5250 cm^{-1}) are also demonstrated in Figure 6G. The blue color was assigned to the higher wavenumber of the peak position with WHB water. Thus, a higher contribution of SHB water in the non-activated eggs than in the activated eggs was revealed (Figure 6G). In summary, the water structural images consistently verified SHB water in the non-activated eggs. It was found that the bioactivity of fish eggs causes significant changes in the water structure and that the water distribution was successfully visualized *in vivo*.

Conclusion

The bioactivity of embryogenesis was assessed through changes in the water structure using NIR spectroscopy and imaging. In the activated eggs after fertilization, the water band at approximately 5250 cm^{-1} shifted to a higher

wavenumber by 2-4 cm^{-1}, and the proportion of WHB water was higher than that in non-activated eggs. The influences of the perturbations to the water structure were evaluated by changing the temperature, ion concentration, protein concentration, and protein secondary structure, and the protein structural transition was revealed to be a possible candidate to induce water structural changes. Actually, in the activated eggs, the protein secondary structure was confirmed to change from an α–helix to a β–sheet rich structure by Raman spectroscopy. The water structure was likely to vary due to the higher proportion of WHB water associated with protein structural changes. The drastic variation in protein components synthesized by gene expression was confirmed, as evaluated from the perspective of water. NIR imaging successfully visualized the dynamic water structural changes depending on the embryogenetic activity. Whether a new life will be born or not was revealed through changes in the water structure.

Acknowledgments

The study was supported by MEXT Leading Initiative for Excellent Young Researchers (M.I.).

Supporting Information

Protocols for the sample preparations, *in vitro* NIR measurements, Raman spectra, supporting figures and table.

References

1. Belyavsky, A.; Vinogradova, T.; Rajewsky, K. *Nucleic Acids Res.* **1989**, *17*, 2919-2932.
2. Ellington, A. D.; Szostak, J. W. *Nature* **1990**, *346*, 818-822.
3. Pandey, A.; Mann, M. *Nature*, **2002**, *405*, 837-846.
4. McKenna, A. et al. *Genome Res.* **2010**, *20*, 1297-1303.
5. Bruchez, M.; Moronne, M.; Gin, P.; Weiss, S.; Alivisatos, A. P. *Science* **1998**, *281*, 2013-2016.
6. Siesler, H. W.; Ozaki, Y.; Kawata, S.; Heise, H. M. (Eds.). *Near-infrared spectroscopy: principles, instruments, applications*, John Wiley & Sons, New Yolk, 2008.
7. Ozaki, Y.; McClure, W. F.; Christy, A. A. (Eds.). *Near-infrared spectroscopy in food science and technology*, John Wiley & Sons, New Yolk, 2006.
8. Ozaki, Y.; Huck, C. W.; Beć, K. B. Near infrared spectroscopy and its applications, in: V. P. Gupta (Ed.), *Molecular and Laser Spectroscopy*, Elsevier, Amsterdam, **2017**, pp.11-38.
9. Heise, H. M. Applications of near-infrared spectroscopy in medical

sciences, in: H. W. Siesler, Y. Ozaki, S. Kawata, H. M. Heise (Eds.), *Near-infrared spectroscopy*, Wiley-VCH, Weinheim, 2002, pp.289.

10. Ozaki, Y. Near-Infrared Spectroscopy – Its Versatility in Analytical chemistry. *Anal. Sci.* **2012**, *28*, 545–563.
11. Ozaki, Y. *Bull. Chem. Soc. Japan* **2019**, *92*, 629-654.
12. Maeda, Y.; Kitano, H. *Spectrochim. Acta A* **1995**, *51*, 2433-2446.
13. Gniadecka, M.; Wessel, S.; Heidenheim, M.; Wulf, H. C.; Nielsen, O. F.; Christensen, D. H. *J. Invest. Dermatol.* **1998**, *111*, 1129-1133.
14. Pettersson, L. G. M.; Henchman, R. H.; Nilsson, A. *Chem. Rev.* **2016**, *116*, 7459-7462.
15. Walrafen, G. E.; Fisher, M. R.; Hokmabadi, M. S.; Yang, W. H. *J. Chem. Phys.*, **1986**, *85*, 6970-6982.
16. Šašic, S.; Segtnan, V. H.; Ozaki, Y. *J. Phys. Chem. A* **2002**, *106*, 760-766.
17. Czarnik-Matusewicz, B.; Pilorz, S.; Hawranek, J. P. *Anal. Chim. Acta* **2005**, *544*, 15-25.
18. Segtnan, V. H.; Šašić, Š.; Isaksson, T.; Ozaki, Y. *Anal. Chem.* **2001**, *73*, 3153-3161.
19. Maeda, H.; Ozaki, Y.; Tanaka, M.; Hayashi, N.; Kojima, T. *J. Near*

Infrared Spec. **1995**, *3*, 191-201.

20. Okajima, H.; Ando, M.; Hamaguchi, H.O. *Bull. Chem. Soc. Japan* **2018**, *91*, 991-997.
21. Luck, W. A. *Ange. Chem. Int. Ed. Engl.* **1980**, *19*, 28-41.
22. Eisenberg, D.; Kauzmann, W. (Eds.). *The structure and properties of water*. Oxford University Press, Oxford, 2005.
23. Salzer, R.; Siesler, H. W. (Eds.). *Infrared and Raman Spectroscopic Imaging*, Wiley-VCH, Weinheim 2nd version, 2014.
24. Šaši´c, S.; Ozaki, Y. (Eds.). *Raman, Infrared, and Near-Infrared Chemical Imaging*, John Wiley & Sons, Inc, New York, 2009.
25. Ishikawa, D.; Shinzawa, H.; Genkawa, T.; Kazarian, S. G.; Ozaki, Y. *Anal. Sci.* **2014**, *30*, 143-150.
26. Ishigaki, M.; Kawasaki, S.; Ishikawa, D.; Ozaki, *Sci. Rep.* **2016**, 6, 20066.
27. Ishigaki, M.; Yasui, Y.; Puangchit, P.; Kawasaki, S.; Ozaki, Y. *Molecules* **2016**, *21*, 1003.
28. Puangchit, P.; Ishigaki, M.; Yasui, Y.; Kajita, M.; Ritthiruangdej, P.; Ozaki, Y. *Analyst* **2017**, *142*, 4765-4772.
29. Ishigaki, M.; Nishii, T.; Puangchit, P.; Yasui, Y.; Huck, C. W.; Ozaki, Y.

J. Biophotonics **2018**, *11*, e201700115.

30. Ishigaki, M. et al. *Anal. Chem.* **2018**, *90*, 5217-5223.
31. Workman Jr, J.; Weyer, L. *Practical guide and spectral atlas for interpretive near-infrared spectroscopy*, CRC Press, Boca Raton, 2012.
32. Holly, S.; Egyed, O.; Jalsovszky, G. *Spectrochim. Acta A: Mol. Spectrosc.* **1992**, *48*, 101-109.
33. Yang, W. Y.; Larios, E.; Gruebele, M. *J. Am. Chem. Soc.* **2003**, *125*, 16220-16227.
34. Robert, P.; Devaux, M. F.; Mouhous, N.; Dufour, E. *Appl. Spectrosc.* **1999**, *53*, 226-232.
35. Miyazawa, M.; Sonoyama, M. *J. Near Infrared Spectros.* **1998**, *6*, A253-A257.
36. W. Hug, J. M. Chalmers and P. R. Griffith, *Handbook of vibrational spectroscopy*, 2002, John Wiley and Son Ltd., Chichester, 2002.
37. Sato, T.; Kawano, S.; Iwamoto, M. *J. Am. Oil Chem. Soc.* **1991**, *68*, 827-833.
38. Holliday, F. G. T.; Jones, M. P. *J. Mar. Biol. Assoc. UK* **1967***, 47*, 39‑48.
39. Wold, S.; Esbensen, K.; Geladi, P. *Chemom. Intell. Lab. Syst.* **1987**, *2*,

37-52.

40. Hofmeister, F. *Arch. Exp. Pathol. Pharmacol.* **1888**, *24*, 247-260.

41. Wu, Y.; Czarnik-Matusewicz, B.; Murayama, K.; Ozaki, Y. *J. Phys. Chem.* **2002**, *104*, 5840.

42. Movasaghi, Z.; Rehman, S.; Rehman, I. U. *Appl. Spectrosc. Rev.* **2007**, *42*, 493-541.

43. Liu, Y.; Cho, R. K.; Sakurai, K.; Miura, T.; Ozaki, Y. *Appl. Spectrosc.* **1994**, *48*, 1249-1254.

44. Izutsu, K. I.; Fujimaki, Y.; Kuwabara, A.; Hiyama, Y.; Yomota, C.; Aoyagi, N. *J. Pharm. Sci.* **2006**, *95*, 781-789.

45. Sato, T. *J. Am. Oil Chem. Soc.* **1994**, *71*, 293-298.

46. Grabska, J.; Ishigaki, M.; Beć, K. B.; Wójcik, M. J.; Ozaki, Y. *J. Phys. Chem. A* **2017**, *121*, 3437-3451.

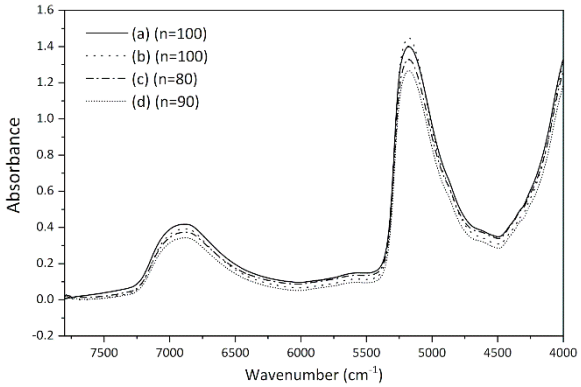

Figure 1: Mean NIR absorbance spectra obtained from four kinds of egg yolk groups.

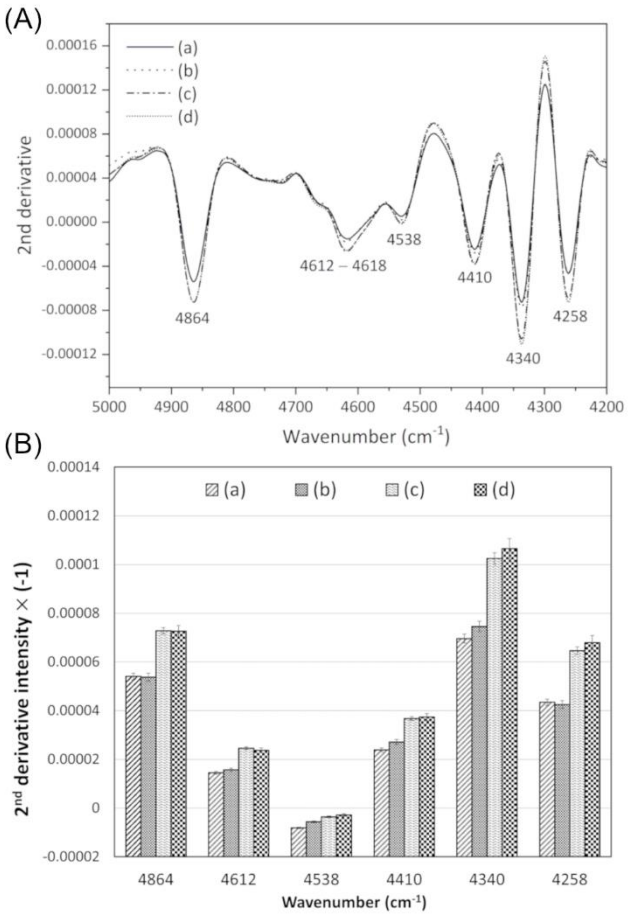

Figure 2: (A) Second derivative of the NIR spectra recorded from the four kinds of egg yolk groups in the 5500-5000 cm^{-1} region. (B) Graphs comparing the second derivative intensities at 4864, 4612, 4538, 4410, 4340, and 4258 cm^{-1} with the standard error (SE).

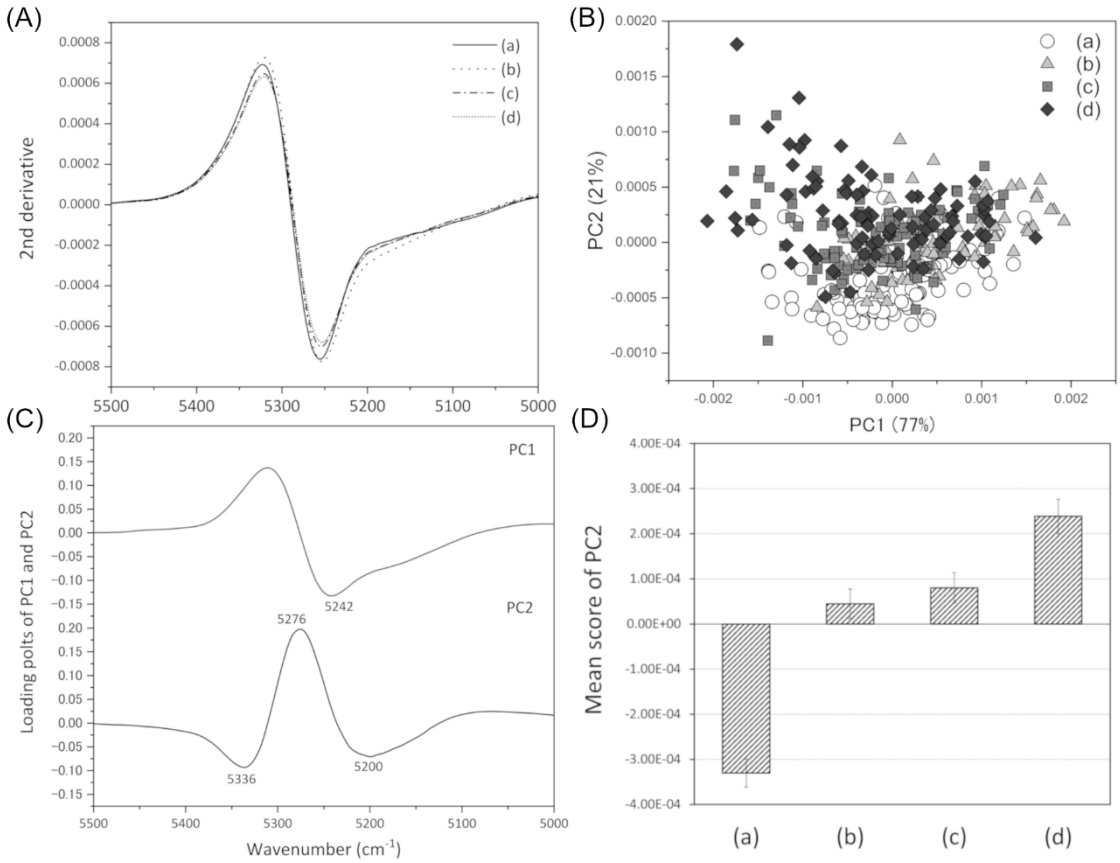

Figure 3: (A) Second derivative NIR spectra recorded from the four kinds of egg yolk groups in the 5500-5000 cm^{-1} region. (B) Score and (C) loading plots of principal component (PC) 1 and PC2. (D) Mean score of PC2 with SE for the four kinds of egg groups.

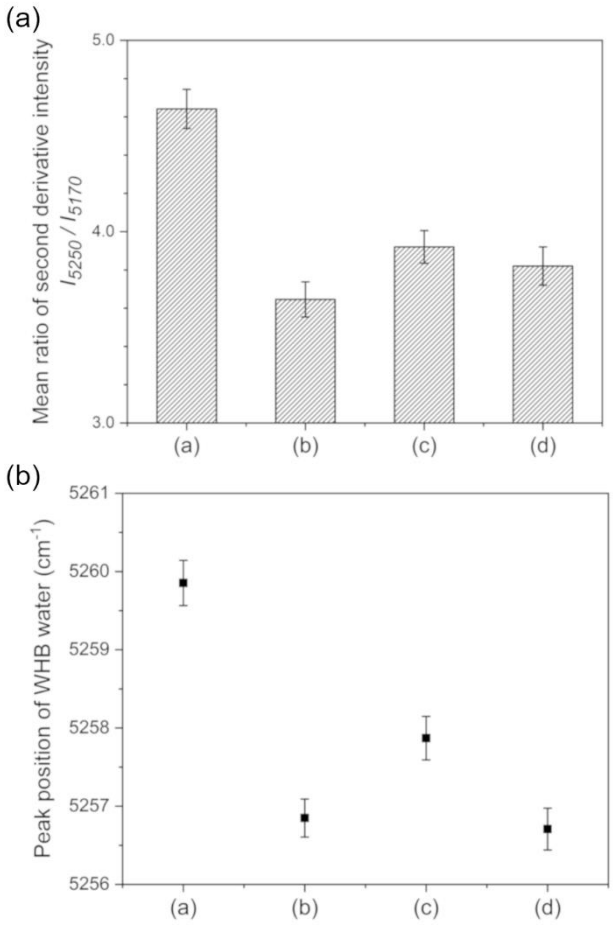

Figure 4: (A) Mean ratio of the second derivative intensities (I_{5250}/I_{5170}) with SE. (B) The wavenumber peak position at approximately 5250 cm^{-1} with SE.

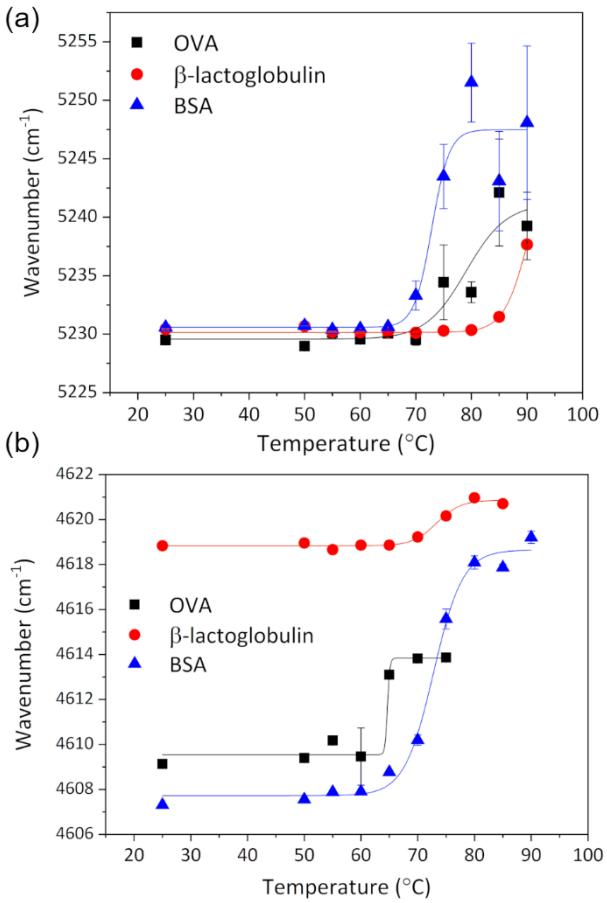

Figure 5: Plots of the band positions of (A) WHB water and (B) proteins at approximately 5250 and 4610 cm^{-1}, respectively, due to the denaturation of ovalbumin (OVA), β-lactoglobulin, and bovine serum albumin (BSA).

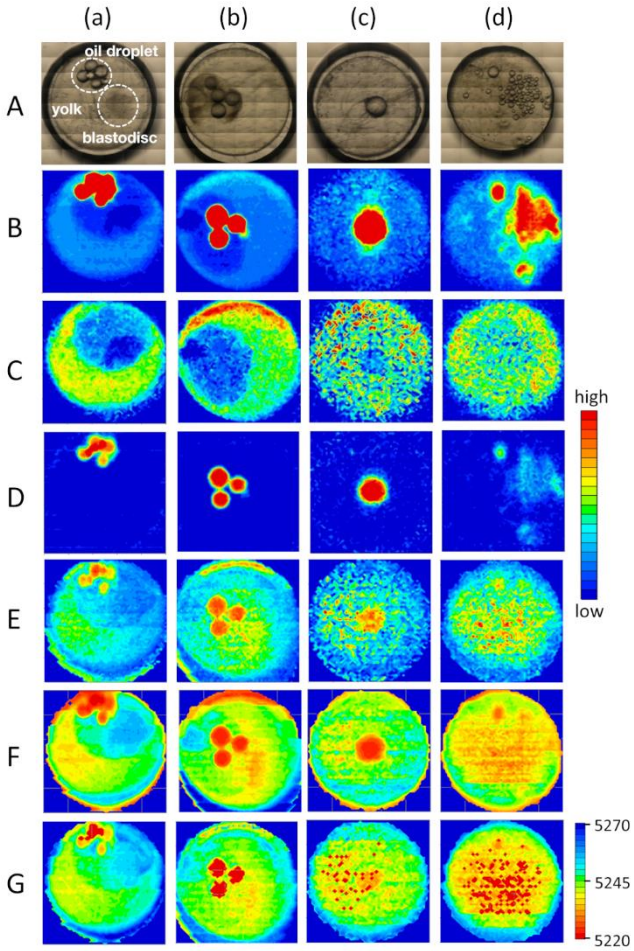

Figure 6: (A) Visible images of the four kinds of fish egg groups. (B)-(D) NIR images constructed by plotting second derivative intensities of the bands at 4340, 4616, and 5856 cm^{-1}, respectively. (E)-(G) NIR images made by plotting (E) the ratio of the second derivative intensities of the water bands defined as I_{5170}/I_{5250}, (F) PC2 scores, and (G) the peak position due to NHB water (~5250 cm^{-1}).

Supporting Information

Assessment of embryonic bioactivity through changes in the water structure using near-infrared (NIR) spectroscopy and imaging

Mika Ishigaki,[1,2]* Yui Yasui,[3] Misato Kajita,[3] Yukihiro Ozaki[3]

[1]*Raman Project Center for Medical and Biological Applications, Shimane University, 1060 Nishikawatsu, Matsue, Shimane 690-8504, Japan*

[2] *Faculty of Life and Environmental Sciences, Shimane University, 1060 Nishikawatsu, Matsue, Shimane 690-8504, Japan*

[3]*School of Science and Technology, Kwansei Gakuin University, 2-1 Gakuen, Sanda, Hyogo 669-1337, Japan*

* Authors to whom correspondence should be sent.

*E-mail: ishigaki@life.shimane-u.ac.jp (M.I.),

Table of Contents

SI 1. Sample preparations and *in vitro* NIR measurements

In order to quantitatively evaluate the magnitude of a water peak shift at approximately 5200 cm^{-1}, four kinds of perturbations were given to the ultrapure water; (i) temperature, (ii) ion concentration, (iii) protein concentration, and (iv) the secondary structural changes of proteins.

(i) Water temperature

The temperatures of ultrapure water (Purelab Ultra, Analytic, Organo Co. Ltd.,Tokyo, Japan) and 1.0 M NaCl (28-2300, Sigma Aldrich, Japan) were changed from 20 to 70 °C by an increment of 5 °C.

(ii) Ion concentration

Stock solutions of 1.0 M NaCl (28-2300, Sigma Aldrich, Japan) and 1.0 M Na_2SO_4 (S9627, Sigma Aldrich, Japan) were diluted with the ultrapure water so as to have solutions with the concentration range of 1.0 – 0.1 M with 0.1 M intervals.

(iii) Protein concentration

Albumin (OVA; 012-09885, from chicken egg, FUJUFILM Pure Chemical Co., Japan) aqueous solutions with the concentrations of 2, 4, 8, 12 16, and 20 wt% were prepared using 0.05 M Tris-HCl buffer (pH=7.6, FUJUFILM Pure Chemical Co., Japan).

(iv) Protein secondary structural changes

Protein samples of OVA, β-lactoglobulin (L3908, from bovine milk,

Sigma-Aldrich Co., USA), and bovine serum albumin (BSA; 013-15121, FUJUFILM Pure Chemical Co., Japan) were diluted in 0.05 M Tris-HCl buffer at 8 wt%. Micro tubes containing 1 mL of each protein solution were heated from 50-90 °C by 5 °C intervals for 20 minutes, cooled with ice water, and subjected to NIR measurements at 25 °C.

For the NIR measurements, a Spectrum One FT-NIR (Perkin-Elmer, Waltham, MA, USA) was used. The optical path length of an open quartz cell was 0.1 or 0.5 mm. The wavenumber region measured was 10000-4000 cm^{-1}, the spectral resolution was 4 cm^{-1}, and the accumulation was 128 times. Every measurement was repeated three times. The temperature of the quartz cell was controlled by a bath circulator (NESLAB RTE7, Thermo Scientific, Waltham, MA, USA). The stability of the temperature was ±0.1 °C.

SI 2. Temperature-dependent NIR spectral variation of pure water

NIR absorbance spectra of the ultrapure water were recorded in the range of 10-80 °C by the increment of 5 °C using a quartz cell with 0.3 mm optical path length (Figure S1A). Absorbance peaks due to the water at approximately 7000 and 5200 cm^{-1} shifted to a higher frequency with an increase in the water temperature. In the second derivative spectra of the absorbance in the 5300-5000 cm^{-1} region, two peaks at 5250 and 5170 cm^{-1} were observed, and their peak intensities became stronger and weaker as the temperature increased, respectively (Figure S1B). Hydrogen bonds between water molecules break as the water temperature increases. Therefore, two

peaks at 5250 and 5170 cm^{-1} can be assigned as weakly hydrogen bonded (WHB) and strongly hydrogen bonded (SHB) water species, respectively. That is, the higher the proportion of WHB water species, the higher the frequency of the water band is.

SI 3. Estimation of the protein weight percentage of an egg

Murakami et al. extracted the total amount of water-soluble proteins in embryos on the 1st day after fertilization as about 12.5 mg/100 eggs on the day after fertilization.[47] Iwamatsu et al. reported the diameter of the egg about 1.2 mm.[48] If the specific gravity of an egg is assumed as 1, the weight percent concentration of water-soluble proteins amounts to the order of 10 wt%.

SI 4. NIR spectral variations caused by protein secondary structural changes

To reveal the NIR spectral variations caused by the protein secondary structural changes, the denaturation processes of OVA, β-lactoglobulin, and BSA were investigated. These three proteins have different proportions of α-helix and β-sheet components; β-lactoglobulin and BSA have β-sheet and α-helix rich structures, respectively, and OVA has a comparable ratio of the two.[49-57] Table S1 summarizes the properties of these three proteins.[49-57] Their protein secondary structures are known to increase the proportion of a

β-sheet at the expense of an α-helix by thermal denaturation,[49-57] and the spectral variations induced by the denaturation were observed in a few marker regions. Figure S2A, S2B, and S2C exhibit the second derivative spectra of the three kinds of proteins in the 4900-4800, 4700-4550, and 4600-4450 cm^{-1} regions, respectively. These three regions have common peaks due to proteins in both the pure protein samples and in fish eggs.

A peak at approximately 4860 cm^{-1} slightly shifted to a lower wavenumber with the thermal denaturation (Figure S2A). Liu et al. reported that denatured pepsin, which originally had a β-sheet rich structure exhibited a higher frequency shift of the amide A/II band in the NIR region in conjunction with an upward shift of amide A in the corresponding IR spectrum.[43] In the structural transition of silk fibroins, the corresponding band was shifted downward from 4875 to 4860 cm^{-1} as reported by Miyazawa et al.[35] Even though the patterns of the band shift depend on the protein species, amide A/II can be a marker band to monitor the variation of hydrogen bonds in amide groups caused by the structural variations of proteins.

The peak at around 4610 cm^{-1} has been reported to be related to an α-helix structure (Figure S2B).[34] Peak intensity at 4610 cm^{-1} of silk fibroin was decreased by thermal denaturation with similar increments to the one at 4520 cm^{-1} that was assigned to a β–sheet structure mentioned below.[35] In the present results shown in Figure S2B, the peak intensities consistently decreased in the β-lactoglobulin and BSA spectra with the thermal

denaturation. In the OVA spectrum, on the other hand, a large peak shift to a higher frequency was observed from 4606 to 4618 cm^{-1}. The other two samples, β-lactoglobulin and BSA, also yielded higher frequency shifts of the corresponding peaks, which may be an indicator for the structural changes of proteins.

In Figure S2C, peaks appeared at 4534 and 4530 cm^{-1} in the spectra of OVA and BSA, respectively, and the peak intensity at 4540 cm^{-1} increased for β-lactoglobulin with an increase of β-sheet components by the thermal denaturation. Proteins that are rich in a β-sheet structure, such as concanavalin and β-lactoglobulin, originally showed clear bands at approximately 4525 cm^{-1}.[35] Robert et al. also assigned the peak at 4535 cm^{-1} as a β-sheet structure based on 12 model proteins.[35] These results indicate that the peak at 4525 cm^{-1} is likely relate with a β-sheet structure.

SI 5. Investigation of protein secondary structural changes in egg yolks using Raman spectroscopy

Figure S3A and S3B depict the mean Raman spectra of the four kinds of groups of eggs (a)-(d) in amide I (~1660 cm^{-1}) and amide III (~1250 cm^{-1}), respectively.[42] In the wavenumber region of amide III, a decrement and an increment of the band intensities were observed at 1268 and 1235 cm^{-1} in activated egg group (a), respectively (Figure S3A). In the amide I region, the Raman band at 1660 cm^{-1} shifted to 1662 cm^{-1}. In both the amide mode regions, the relative proportion of the protein components with an α-helix

and a β-sheet structures were decreased and increased, respectively.[42]

For Raman spectral acquisition of the four kinds of fish egg yolks, the *inVia* confocal Raman microscope (Renishaw Inc., UK) system with an excitation of 785 nm and an objective lens (20×) were used. The Raman spectra were recorded in the 1700-600 cm^{-1} region with an exposure time of 30 s and 2 scan accumulations; the laser power at the sample point was about 3 mW. Ten spectra for each egg were obtained and the procedure was repeated for several different eggs in each egg group. The obtained Raman spectra were preprocessed by background subtraction, baseline correction with 5^{th} order polynomial fitting, and normalization using the phenylalanine band intensity at 1003 cm^{-1}.

Table S1: Properties of three kinds of proteins; ovalbumin (OVA), β-lactoglobulin, and bovine serum albumin (BSA).

	OVA	β-lactoglobulin	BSA
α-helix (%)	41	15	66
β-sheet (%)	34	54	3
Molecular Weight	45000	18400	66500
Thermal Denaturation Temperature (℃)	78	70	62-64

(A)

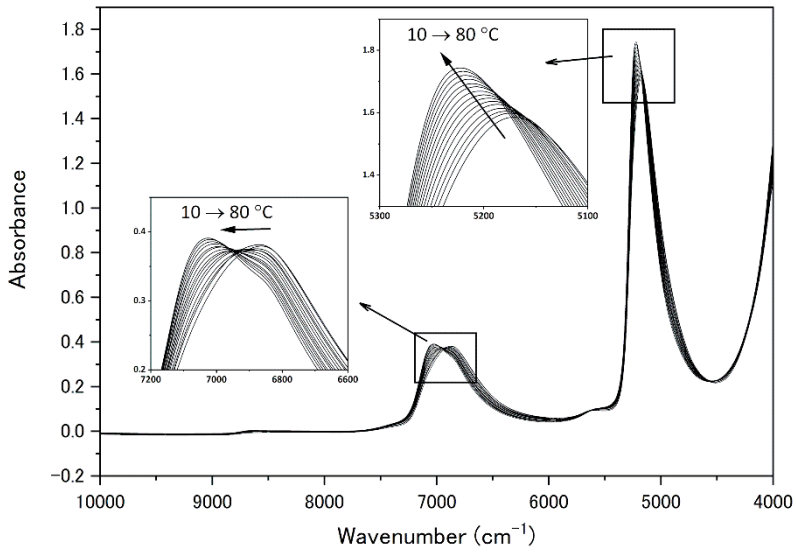

(B)

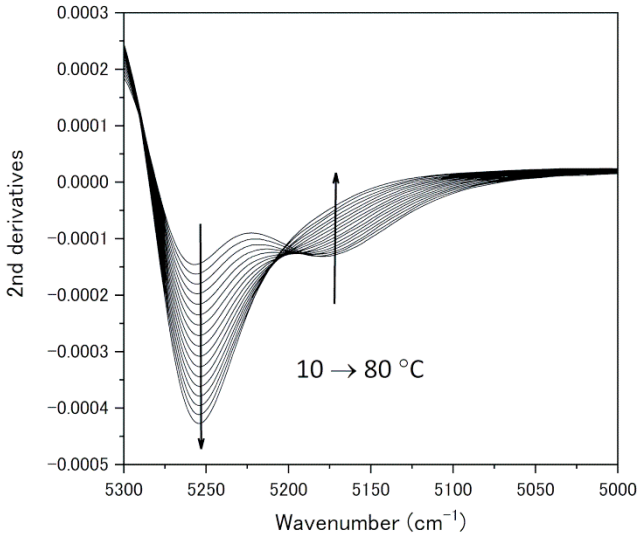

Figure S1: (A) Temperature dependent NIR absorbance spectra of the ultrapure water in the range of 10-80 °C by 5 °C interval. (B) The second derivative spectra in the 5300-5000 cm^{-1} region.

(A)

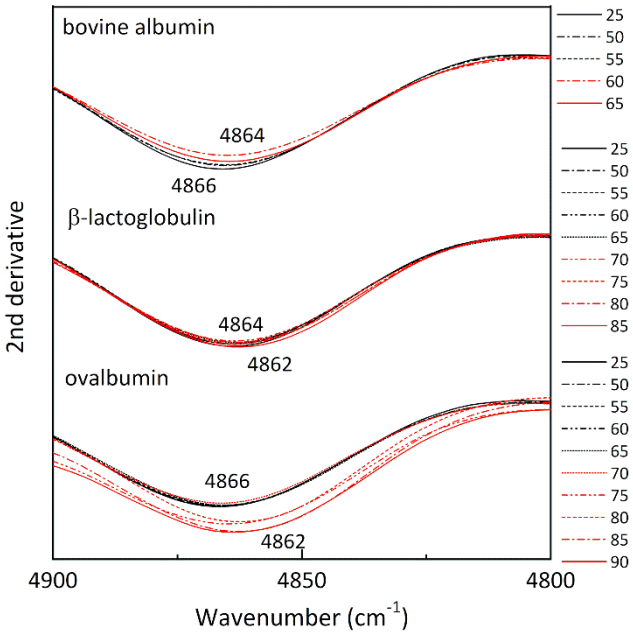
bovine albumin
4864
4866
β-lactoglobulin
4864
4862
ovalbumin
4866
4862
2nd derivative
4900
4850
4800
Wavenumber (cm-1)
25
50
55
60
65
70
75
80
85
90

(B)

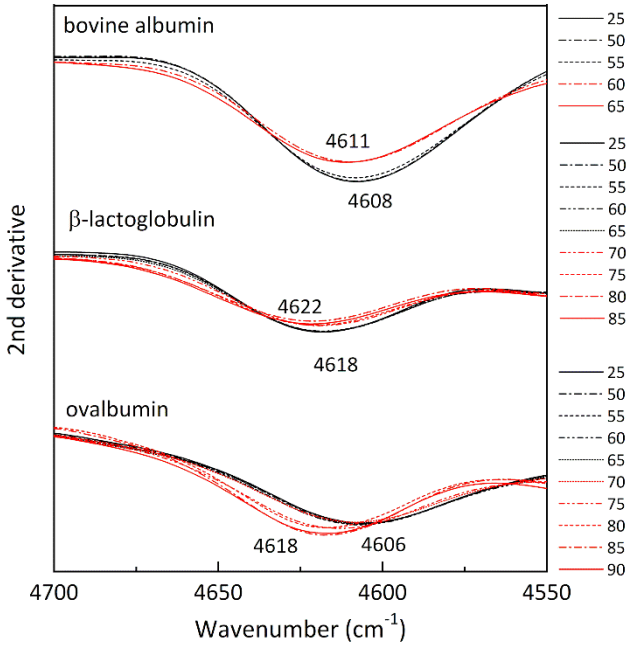
bovine albumin
4611
4608
β-lactoglobulin
4622
4618
ovalbumin
4618
4606
2nd derivative
4700
4650
4600
4550
Wavenumber (cm-1)
25
50
55
60
65
70
75
80
85
90

(C)

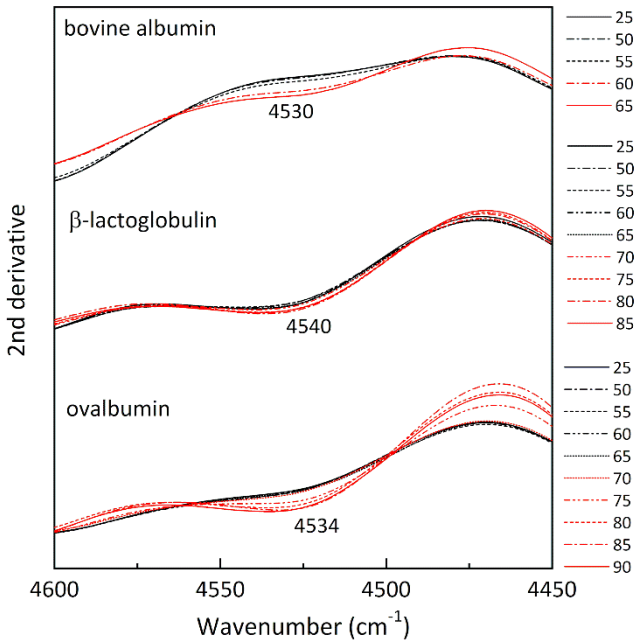

Figure S2: Temperature-dependent variations in the second derivative spectra of ovalbumin (OVA), β-lactoglobulin, and bovine serum albumin (BSA) in the (A) 4900-4800 cm^{-1}, (B) 4700-4550 cm^{-1} and (C) 4600-4450 cm^{-1} regions.

(A)

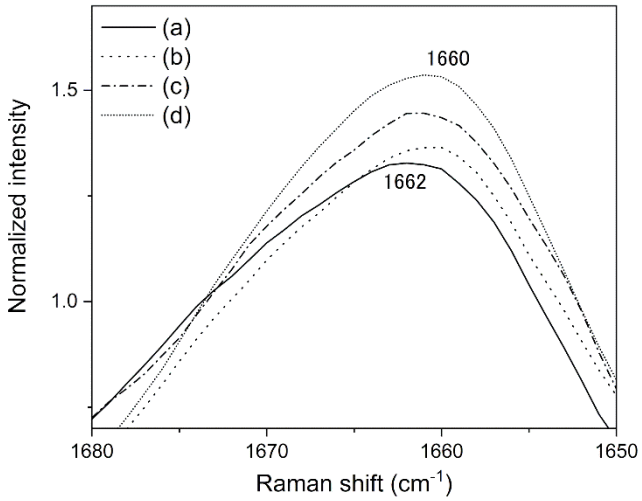

(B)

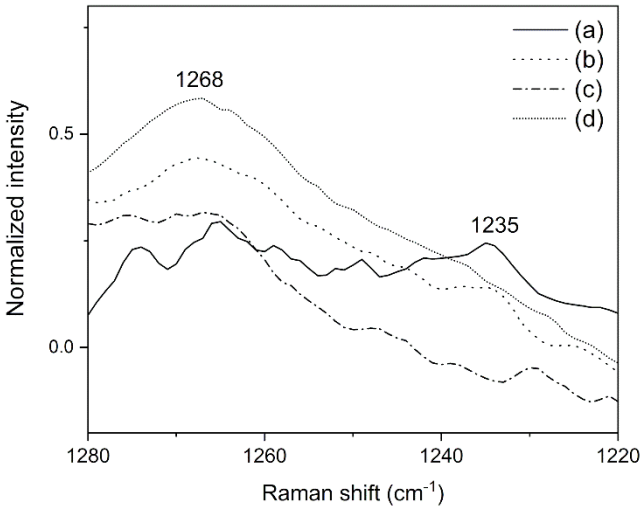

Figure S3: Raman spectra of the four kinds of egg yolks in (A) amide I and (B) amide III regions.

References

47. Murakami, M.; Iuchi, I.; Yamagami, K. *Dev. Growth Differ.* **1990**, *32*, 619-627.
48. Iwamatsu, T. *Mech. Dev.* **2004**, *121*, 605-618.
49. Ngarize, S.; Herman, H.; Adams, A.; Howell, N. *J. Agr. Food Chem.* **2004**, *52*, 6470-6477.
50. Yuan, B.; Murayama, K.; Wu, Y.; Tsenkova, R.; Dou, X.; Era, S.; Ozaki, Y. *Appl. Spectrosc.* **2003**, *57*, 1223-1229.
51. Furlan, P. Y.; Scott, S. A.; Peaslee. M. H. *Spectrosc. Lett.* **2007**, *40*, 475-482.
52. Peters Jr, T. (Ed.). *All about albumin: biochemistry, genetics, and medical applications*, Academic press, 1995.
53. Peters Jr, T. *Serum albumin*, In: C. B. Anfinsen, J. T. Edsall, F. M. Richards (Eds.), *Advances in protein chemistry*, Academic Press **1985**, *37*, 161-245.
54. De Wit, J. N.; Swinkels, G. A. M. *Biochim. Biophys. Acta Protein Struct.* **1980**, *624*, 40-50.
55. Papiz, M. Z.; Sawyer, L.; Eliopoulos, E. E.; North, A. C. T.; Findlay, J. B. C.; Sivaprasadarao, R.; Jones, T. A.; Newcomer, M. E.; Kraulis, P. J. *Nature* **1986**, *324*, 383-385.
56. Rüegg, M.; Moor, U.; Blanc, B. *J. Dairy Res.* **1977**, *44*, 509-520.
57. Harmsen, B. J. M.; Breem, W. J. M. *Int. J. Protein Res.* **1969**, *1*, 225-233.